

Hemodynamics of aneurysm intervention with different stents

Peichan Wu(吴镔婵), Yuhan Yan(严妤函), Huan Zhu(朱欢), Juan Shi(施娟), and Zhenqian Chen(陈振乾)

Citation: Chin. Phys. B, 2022, 31 (**6**): 064701. DOI: 10.1088/1674-1056/ac5603
Journal homepage: http://cpb.iphy.ac.cn; http://iopscience.iop.org/cpb

What follows is a list of articles you may be interested in

Effect of viscosity on stability and accuracy of the two-component lattice Boltzmann method with a multiple-relaxation-time collision operator investigated by the acoustic attenuation model

Le Bai(柏乐), Ming-Lei Shan(单鸣雷), Yu Yang(杨雨), Na-Na Su(苏娜娜), Jia-Wen Qian(钱佳文), and Qing-Bang Han(韩庆邦)

Chin. Phys. B, 2022, 31 (**3**): 034701. DOI: 10.1088/1674-1056/ac2b93

Comparative investigation of microjetting generated from monocrystalline tin surface and polycrystalline tin surface under plane impact loading

Shao-Wei Sun(孙少伟), Guan-Qing Tang(汤观晴), Ya-Fei Huang(黄亚飞), Liang-Zhi Cao(曹良志), and Xiao-Ping Ouyang(欧阳晓平)

Chin. Phys. B, 2021, 30 (**10**): 104701. DOI: 10.1088/1674-1056/abeeea

Effect of non-condensable gas on a collapsing cavitation bubble near solid wall investigated by multicomponent thermal MRT-LBM

Yu Yang(杨雨), Ming-Lei Shan(单鸣雷), Qing-Bang Han(韩庆邦), and Xue-Fen Kan(阚雪芬)

Chin. Phys. B, 2021, 30 (**2**): 024701. DOI: 10.1088/1674-1056/abbbf8

Alternative constitutive relation for momentum transport of extended Navier-Stokes equations

Guo-Feng Han(韩国锋), Xiao-Li Liu(刘晓丽), Jin Huang(黄进), Kumar Nawnit, and Liang Sun(孙亮)

Chin. Phys. B, 2020, 29 (**12**): 124701. DOI: 10.1088/1674-1056/abb3e5

Effects of thiocyanate anions on switching and structure of poly(N-isopropylacrylamide) brushes

Xin-Jun Zhao(赵新军), Zhi-Fu Gao(高志福)

Chin. Phys. B, 2019, 28 (**6**): 064701. DOI: 10.1088/1674-1056/28/6/064701

Hemodynamics of aneurysm intervention with different stents

Peichan Wu(吴锆婵)[1,†], Yuhan Yan(严妤函)[2,†], Huan Zhu(朱欢)[3], Juan Shi(施娟)[1,‡], and Zhenqian Chen(陈振乾)[1]

[1] *School of Energy and Environment, Southeast University, Nanjing* 210096, *China*
[2] *Department of Geriatrics, General Hospital of Eastern Theater Command, Nanjing* 210002, *China*
[3] *Department of Pediatrics, Zhongda Hospital, Southeast University, Nanjing* 210009, *China*

(Received 1 November 2021; revised manuscript received 31 January 2022; accepted manuscript online 17 February 2022)

An ideal cerebral aneurysm model with different stent forms is established. By using the single-relaxation-time (SRT) lattice Boltzmann method (LBM) to solve the flow field, the blood flow characteristics in the aneurysm under different conditions are studied numerically. The intra-arterial stenting of saccular aneurysms at different Reynolds numbers and the feasibility of new stenting forms such as double stenting and variable-spacing stenting in the aneurysms are explored. The hemodynamic factors such as velocity distribution and wall shear stress (WSS) in the aneurysm are analyzed. Numerical results show that the risk of aneurysm rupture is mainly centralized at the right corner of the aneurysm. Intervention of stents in the aneurysm can effectively reduce the intra-aneurysmal velocity and WSS, and decrease the danger of aneurysm rupture during strenuous exercise or emotional excitement. At the same time, the intervention of a double stent and the stent shape with a dense anterior part in the aneurysm has certain advantages in preventing aneurysm rupture. The intra-aneurysmal mean velocity reduction can reach 90.39% and 80.29% after the intervention of the double stent and the anterior densified stent respectively.

Keywords: aneurysm, hemodynamics, stent, lattice Boltzmann method

PACS: 47.63.–b, 47.15.–x, 47.60.Dx, 47.11.–j **DOI:** 10.1088/1674-1056/ac5603

1. Introduction

According to the "2020 World Health Statistics Report" published by the World Health Organization, the death rate of cardiovascular and cerebrovascular diseases ranks first in the proportion of deaths from non-communicable diseases, higher than that of cancer and other diseases. In cardiovascular and cerebrovascular diseases, intracranial aneurysm threatens human health. Due to its complex shape and special location, it has attracted extensive attention from medical workers, patients themselves and scholars at home and abroad.[1] Research statistics show that in the United States, 6 million people have unruptured aneurysms in their brains, while about 3×10^4 people have ruptured; one in every 50 people has a ruptured intracranial aneurysm, and 1 case of intracranial aneurysm rupture occurs every 18 minutes.[2] The high morbidity and mortality rates make it particularly important to detect intracranial aneurysms early and monitor them to prevent the rupture of the aneurysm.

Therefore, more and more studies have begun to focus on indicators that can better predict aneurysm rupture.[3] Among all the risk factors involved, the hemodynamics of the aneurysm is considered to be the most basic one. Numerous previous studies have shown that hemodynamic parameters such as blood flow velocity, wall shear stress (WSS), pressure and blood flow pattern are closely related to the initiation, growth and rupture of intracranial aneurysms.[4–6] Abdullah *et al.*[7] studied the physiological flow of a patient-specific cerebral aneurysm model under resting and exercise conditions. It was concluded that excessively high blood pressure and blood flow velocity under exercise conditions would cause abnormal wall pressure and WSS distribution, making the aneurysm wall easier to rupture. Meng *et al.*[8] believed that "the dispute between high and low WSS" was a manifestation of the complexity of the pathophysiology of aneurysms. Both high and low WSS could drive the growth and rupture of intracranial aneurysms. High WSS would cause the destruction of the elastic membrane in the blood vessel wall, leading to remodeling of the vessel wall; while low WSS would cause the destruction of the endothelial cell gap in the artery, resulting in the remodeling of the endothelial cell wall and even cell apoptosis, which led to the rupture of the aneurysm. Marcello *et al.*[9] sorted out the most commonly used hemodynamic parameters in aneurysm assessment, including WSS, relative residence time (RRT), oscillatory shear index (OSI), *etc.* It was pointed out that selecting appropriate aneurysm rupture indicators was of great significance for predicting aneurysm rupture.

In addition, studying the intra-aneurysm hemodynamics is helpful for clinicians to formulate a reasonable treatment plan for patients with intracranial aneurysms. Stents are currently a relatively mature treatment method in improving

[†]These authors contributed equally to this work.
[‡]Corresponding author. E-mail: Shi_juan@seu.edu.cn

© 2022 Chinese Physical Society and IOP Publishing Ltd

the hemodynamic environment within the aneurysm.[10] The shunt stent can be regarded as a kind of porous medium,[11] which can play the role of blood diversion. It is effective in improving the blood flow within the aneurysm-carrying artery, for the purpose of stopping the aneurysm from continuing to grow or rupture.[12] Many current studies are dedicated to investigate the hemodynamic effects of different stent forms on aneurysms. Zhang *et al.*[13] studied the hemodynamic performance of overlapping bare stents in the interventional treatment of thoracic aortic aneurysm (TAA). The results showed that the overlapping stent intervention reduced the pressure acting on the capsule wall, and the pressure distribution became more uniform, thereby protecting the aneurysm from rupture. Suri *et al.*[14] proposed a new method of manufacturing a variable porosity stent. The stent contained a low-porosity sheet-like area that covered the neck of the aneurysm and blocked the blood flow into the aneurysm, thus achieving embolization without endangering nearby perforating vessels. Chen *et al.*[15] described four stent models with different pole geometries (circle, triangle, hexagon, and spline). Their analysis showed that the hexagonal geometry was a relatively good support design. To further improve the application research of stents in the treatment of interventional aneurysms, it can provide certain help to the treatment of aneurysms.

Due to the complex geometry of the aneurysm and its physiological environment, the use of existing clinical observations, animal experiments and *in vitro* experiments is subject to many restrictions. The experimental conditions are demanding, and the flow parameters that can be obtained in the experiment are limited. Computational fluid dynamics (CFD) provides a new way for numerical simulation of hemodynamics.[16] Lattice Boltzmann method (LBM) is popular in calculating various fluid flow problems. Compared with other traditional CFD methods, it has the benefits of simple fluid interaction description, easy setting of complex boundaries, easy parallel calculation, and easy implementation of programs.[17–19] In recent years, LBM has been systematically adopted in several computational hemodynamic applications, such as blood flow simulation in blood vessels,[20,21] heart valves,[22] aneurysms,[23] and aorta.[24]

A large number of scholars have carried out research on the hemodynamic mechanism in aneurysms through LBM. The effects of different vessel locations, aneurysm shapes, and changes in hemodynamic parameters have been explored. Some studies have also verified the practical application effects of different forms of stents in the interventional treatment of cranial aneurysms.

Osaki *et al.*[25] performed a lattice Boltzmann simulation of the flow in cerebral aneurysm model by using single-, two-, and multiple-relaxation-time collision models. It was concluded that single-relaxation-time model gave reasonable predictions similar to multiple-relaxation-time model. Afrouzi *et al.*[26] studied the simulation of blood flow in saccular and cloacal aneurysms that commonly occurred on the arterial wall, considering the effect of non-Newtonian blood in the model. Different flow patterns and analysis of hemodynamic factors were acquired. Czaja *et al.*[27] investigated the effect of pulsatile blood flow on red blood cells (RBCs) and platelet transport into aneurysm geometries with different dome to neck aspect ratios. As the aspect ratio increases, the average aneurysm velocity decreased, and aneurysms with higher aspect ratios were likely to have greater thrombosis. Chopard *et al.*[28–30] studied the performance of the screen-model-based approach for stents under various conditions, such as placing different stents in the artery, different homogeneous porosity and different pulsating entrance velocities. The test results highlighted the effectiveness of this model in the treatment of common aneurysms with shunt stents on a large scale. Zhang *et al.*[31] focused on the association between porosity configuration and scaffold efficacy. Four patient-specific intracranial aneurysm geometries were used to perform LBM simulations of interventional stents with different porosity. The simulation showed that when the porosity was less than 86%, the blood flow in the intracranial aneurysm sac was significantly reduced; when the porosity was less than 70%, the stent was likely to cause thrombus formation in the patient's blood vessel.

In summary, at present, the stent application problem for the preferred form of the stent is still under exploration. There are few studies on considering the characteristics of blood flow in aneurysms under different conditions, as well as new stent forms such as double stents and variable spacing stents. In this paper, ideal cerebral aneurysm models with different stent shapes are established, and LBM is applied to numerically study the flow characteristics in the aneurysm under resting and exercise conditions. At the same time, the feasibility of new stents such as double stents and variable-spacing stents is considered. Hemodynamic factors such as blood flow velocity distribution characteristics and WSS within the saccular aneurysm will be analyzed and compared.

2. Numerical methods

2.1. Lattice Boltzmann model

The nine-velocity incompressible lattice Bhatnagar–Gross–Krook (BGK) model (D2Q9) for the two-dimensional study proposed by Guo *et al.*[32] is adopted in the present simulation. The evolution of this method can be expressed by the following equation:

$$\begin{aligned} & f_\alpha(\boldsymbol{x}+\boldsymbol{e}_\alpha\delta t, t+\delta t) - f_\alpha(\boldsymbol{x},t) \\ &= -\frac{1}{\tau}\left[f_\alpha(\boldsymbol{x},t) - f_\alpha^{(\mathrm{eq})}(\boldsymbol{x},t)\right], \quad \alpha = 0,1,\ldots,8, \end{aligned} \tag{1}$$

where $f_\alpha(\boldsymbol{x},t)$ is the density distribution function, which represents the mass point moving at the speed $\boldsymbol{e}_\alpha$ at the spatial position $\boldsymbol{x}$ and time t. The dimensionless relaxation time τ is related to the kinematic viscosity coefficient ν, which is defined as

$$\nu = c_s^2\left(\tau - \frac{1}{2}\right)\delta_t, \tag{2}$$

where $c_s = c/\sqrt{3}$ is the lattice sound speed, $c = \delta_x/\delta_t$ is the particle velocity, δ_x and δ_t stand for the time and space increments. $f_\alpha^{(\mathrm{eq})}(\boldsymbol{x},t)$ represents the equilibrium distribution, which can be expressed as

$$f_\alpha^{(\mathrm{eq})} = w_\alpha \rho\left[1 + \frac{\boldsymbol{e}_\alpha\cdot\boldsymbol{u}}{c_s^2} + \frac{(\boldsymbol{e}_\alpha\cdot\boldsymbol{u})^2}{2c_s^4} - \frac{\boldsymbol{u}^2}{2c_s^2}\right],$$
$$\alpha = 0,1,\ldots,8, \tag{3}$$

where w_α is the weight coefficient, which is 4/9 for w_0, 1/9 for $w_{1\text{–}4}$, and 1/36 for $w_{5\text{–}8}$. And for the D2Q9 model, the discrete velocity space for the particle $\boldsymbol{e}_\alpha$ satisfies the following equation:

$$\boldsymbol{e}_\alpha = \begin{cases} (0,0), & \alpha = 0, \\ c\left(\cos\left[(\alpha-1)\dfrac{\pi}{2}\right], \sin\left[(\alpha-1)\dfrac{\pi}{2}\right]\right), & \alpha = 1,2,3,4, \\ \sqrt{2}c\left(\cos\left[(2\alpha-1)\dfrac{\pi}{4}\right], \sin\left[(2\alpha-1)\dfrac{\pi}{4}\right]\right), & \alpha = 5,6,7,8. \end{cases} \tag{4}$$

From the distribution function, the macroscopic density, velocity and pressure can be calculated, expressed as

$$\rho = \sum_\alpha f_\alpha, \quad \rho\boldsymbol{u} = \sum_\alpha \boldsymbol{e}_\alpha f_\alpha, \quad p = c_s^2\rho. \tag{5}$$

The intracranial aneurysm studied in this paper is located in a vessel with a large internal diameter, besides both the fluid velocity and shear velocity are high. Since the non-Newtonian fluid characteristics of blood are presented when the diameter of the blood vessel is less than 1 mm,[26] the study in this work regards blood as Newtonian fluid. In addition, WSS is an important indicator to measure the risk of intracranial aneurysm rupture. The calculation expression of wall shear stress of incompressible Newtonian fluid given in Ref. [33] is referred to in this article. The expression is

$$\tau_i = -\frac{\mu\tau}{c_s^2\rho} f_\alpha^{\mathrm{neq}} e_{\alpha j} n_j (e_{\alpha i} - e_{\alpha k} n_i n_k), \quad i,j,k = 0,1, \tag{6}$$

where μ is the dynamic viscosity, ρ is the fluid density, n_i represents the i-th component of the wall normal vector $\boldsymbol{n}$, and $e_{\alpha i}$ represents the i-th component of the lattice vector $\boldsymbol{e}_\alpha$. $\boldsymbol{n}$ is the unit normal vector at the wall, which can be obtained by $\boldsymbol{n}\cdot\boldsymbol{u} = 0$, $\boldsymbol{u}$ is the macroscopic velocity.

2.2. Physical model and boundary conditions

The physical model of aneurysm used in this study is similar to the model selected by the predecessors when studying this type of problem.[34] Figure 1 shows the 2D calculation model of intracranial aneurysm hemodynamic simulation in this paper. The calculation domain used in the simulation is set as 800×350 ($L_x \times L_y$) lattice. The selected blood vessel diameter D is 80 lattice. The center of the aneurysm is placed at $(L_x/2, h+D)$, where h is the height from the center of the aneurysm to the upper wall of the tumor-bearing vessel. In this model, h is the 108 lattice. The diameter d_0 of the aneurysm model is 200 lattice, the width d_a of the aneurysm mouth is 100 lattice, and the transition chamfer radius r_n at the corners of the aneurysm is 10 lattice. In the calculation, the relaxation time τ is 0.578, the average density ρ is 1.0, and the viscosity coefficient ν is 0.026. The blood is set to flow in from the left vessel along the blood flow direction in Fig. 1. The outer part of the flow field is set as the solid part. The non-equilibrium extrapolation format is adopted at the inlet and outlet boundaries of the flow field, and the rebound format is adopted at the solid boundary.[35]

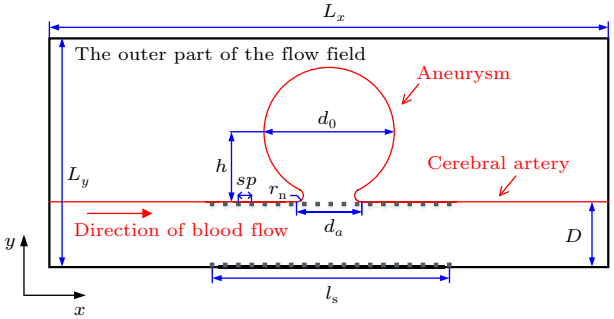


Fig. 1. Physical model of intracranial aneurysm.

The vascular stent in the work is simplified into multiple solid squares with a length of 2 lattices. The horizontal spacing between squares is expressed as *sp* (stent space). The concept of stent porosity ε is used to describe the sparsity of the stent mesh. The bottom of the stent is connected to the bottom solid wall, and the top of the stent is connected to the upper wall of the vessel wall. The stent is inserted into the neck of the aneurysm. The length of the stent l_s is 600 lattices. According to the research content of this work, single-layer stent, double stent, and variable-spacing stent are inserted into the model respectively, as shown in Fig. 2. The double bracket adopts the

mode of alternately building up and down single-layer brackets. For the variable-spacing stent, the fixed aneurysm neck segment S is selected, and the variable-spacing setting of the stent is performed by changing the four structural parameters of sp_1, sp_2, sp_3, and sp_4. Table 1 shows the parameters of the aneurysm interventional stent model used in different groups in this paper. Among them, $sp = sp_1$ is defined as the single-layer stent, $sp = \infty$ is defined as no stent, $sp = sp_1 - sp_2$ is defined as the double stent, and $sp = sp_1 - sp_2 - sp_3 - sp_4$ is defined as the variable-spacing stent.

Table 1. Parameters of aneurysm interventional stent model.

Sample name	Stent shape	
	sp	ε (%)
Single-layer stent ($sp = sp_1$)		
C0	∞	–
C1	35	94.2%
C2	30	93.3%
C3	25	92%
C4	15	86.67%
Double stent ($sp = sp_1$-sp_2)		
C5	30-30	93.3%
Variable-spacing stent ($sp = sp_1$-sp_2-sp_3-sp_4)		
C6	15-22-28-35	92%
C7	35-22-15-28	92%
C8	35-28-22-15	92%

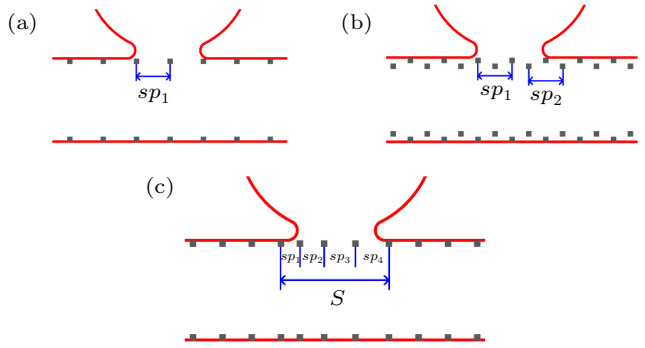


Fig. 2. Stent models for intervention in aneurysm: (a) single-layer stent, (b) double stent, (c) variable-spacing stent.

2.3. Model verification

Before studying specific issues, it is necessary to verify the effectiveness of the LBM model for simulating aneurysms. Here the model of Hirabayashi *et al.*[34] is used for validation. The diameter of the aneurysm d_0 is set as 100 lattices, the width d_a of the aneurysm mouth is 100 lattices, that is, $d_0/d_a = 1$, and h is 58 lattices. The stent is a single-layer stent with a circular cross section of diameter 2, and $sp = 35$, that is, the porosity of the stent is 95.91%. The Reynolds number is defined as $Re = UD/\nu$, where U is the average inlet velocity.[1] When simulating the flow, the Re is set as 300, and the pressure gradient $\mathrm{d}p/\mathrm{d}x$ is 4.17×10^{-6}. This aneurysm model is numerically simulated, and the velocity at the neck of the aneurysm is compared and verified with the results of Hirabayashi *et al.*, as shown in Fig. 3. It can be seen that the calculation results are basically consistent with the results of the existing literature. Therefore, the numerical model is reliable when simulating the flow phenomenon in an aneurysm.

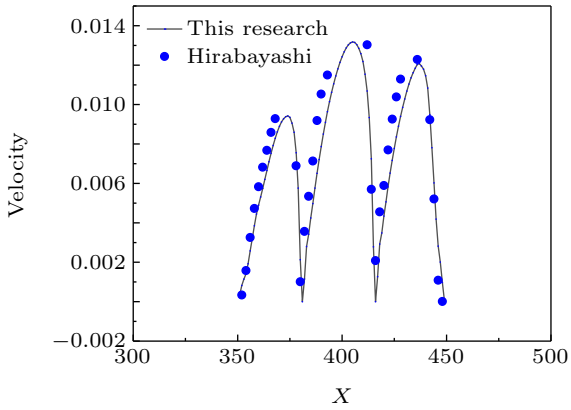


Fig. 3. Comparison of the aneurysm neck velocity in this paper and in Ref. [34].

3. Results and discussion

3.1. Intra-aneurysm hemodynamic analysis during rest and exercise

In this section, the blood flow in the aneurysm when the human body is in a state of rest and exercise is simulated. The purpose of increasing the Reynolds number is achieved by reducing the relaxation factor τ in the lattice Boltzmann model. The Reynolds number at rest is selected as 300, and at exercise is selected as 600.[7] C0, C1, and C4 samples are used to compare the flow characteristics of different stent shapes in aneurysms under different Reynolds numbers.

Figure 4 shows the fluid velocity cloud diagram and flow pattern under different Reynolds number conditions when different stent forms are inserted into aneurysms. As can be seen from Fig. 4(a), the streamlines in the aneurysm are swirling. The fluid flows in from the right aneurysm corner of the aneurysm, and flows out from the left aneurysm corner. The velocity shock at the right aneurysm corner is greater than that at the left aneurysm corner. The greater the speed, the greater the risk of aneurysm rupture.[7] At the same time, comparing Fig. 4(a) with Fig. 4(c), there is a big difference before and after the intervention of the stent in the aneurysm. After the intervention of the stent, the velocity distribution at the aneurysm opening can be significantly improved, and the risk of aneurysm rupture is reduced. Figures 4(c) and 4(e) have been analyzed to show that the smaller the porosity of the interventional stent, the higher the vortex center within the aneurysm and the lower the velocity at the aneurysm orifice. Through the cloud diagrams under different Reynolds number states (Figs. 4(a) and 4(b)), it can be obtained that when the Reynolds number increases, the intra-aneurysmal velocity increases. It can be seen from Fig. 4(b) that due to the increase

in Reynolds number, a vortex appears on the right wall surface of the aneurysm. The flow pattern has changed, and the reflux area in the aneurysm is suppressed. The situation can be improved after the intervention of the stent (see Figs. 4(d) and 4(f)).

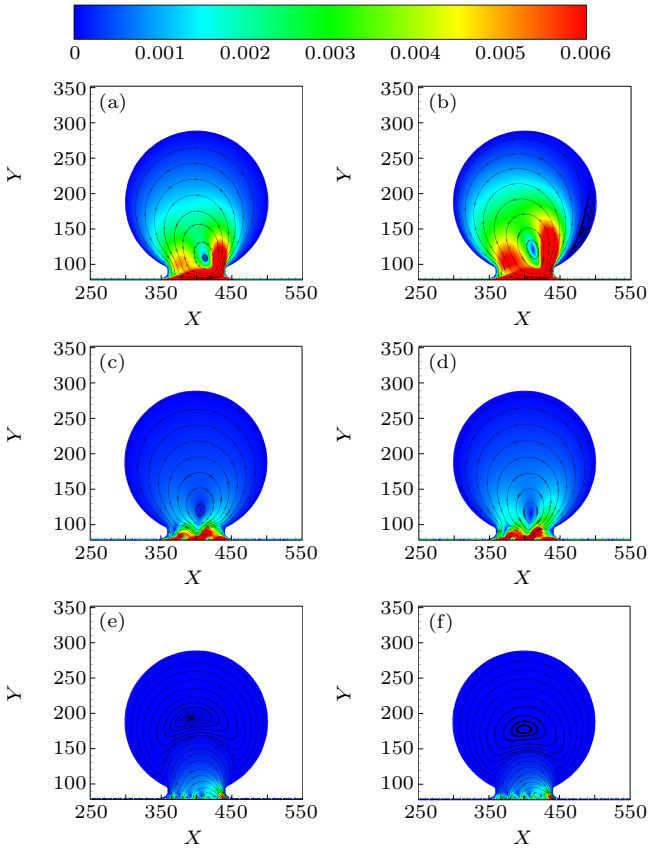


Fig. 4. The flow patterns of different stent shapes in the aneurysm under different Reynolds numbers: (a) $Re = 300$, C0($sp = \infty$); (b) $Re = 600$, C0($sp = \infty$); (c) $Re = 300$, C1($sp = 35$); (d) $Re = 600$, C1($sp = 35$); (e) $Re = 300$, C4($sp = 15$); (f) $Re = 600$, C4($sp = 15$).

In order to quantitatively evaluate the effect of stent intervention in the aneurysm, the intra-aneurysmal velocity reduction V_r is used as a measurement index,[33] which is defined as

$$V_r = \frac{V_n - V_s}{V_n} \times 100\%, \tag{7}$$

where V_n is the average velocity in the aneurysm without stent intervention and V_s is the average velocity with stent intervention.

Table 2 shows the average velocity and velocity reduction within the aneurysm at different Reynolds numbers. It is obvious that the greater the Reynolds number, the greater the velocity within the aneurysm. The interventional stent effectively slows down the blood flow in the aneurysm. The smaller the porosity of the stent, the greater the decrease in intra-aneurysmal velocity. For different Reynolds numbers, the intra-aneurysmal velocity reduction can reach 68% after stenting with a single layer of $sp = 35$ and more than 92% after stenting with $sp = 15$. This greatly reflects the effectiveness of stent therapy.

It can be seen from Fig. 4 that the velocity changes in the aneurysm are centralized at the aneurysm mouth. Therefore, figure 5 shows the aneurysm neck velocity curve when different stent shapes are inserted into the aneurysm under different Reynolds numbers. From Fig. 5, the velocity gradient at the right corner of the aneurysm is larger than that at the left corner, that is, the risk of rupture at the right corner of the aneurysm is higher. After the intervention of the stent, the blood flow velocity at the neck of the aneurysm significantly decreased. It can be found that the stent is an effective treatment to improve the blood flow in the aneurysm. And the lower the porosity of the interventional stent, the lower the blood flow velocity. By comparing the aneurysm neck velocity curves with different Reynolds numbers, it is concluded that the blood flow velocity at the aneurysm neck increases as the Reynolds number increases. When the porosity of the interventional stent becomes smaller, the speed difference between different Reynolds numbers becomes smaller, that is, the low-porosity stent can more effectively improve the blood flow velocity at the neck of the aneurysm.

Table 2. Decrease of intra-aneurysm velocity at different Reynolds numbers.

	Average velocity V	Velocity reduction V_r
$Re = 300$		
C0($sp = \infty$)	0.001616	–
C1($sp = 35$)	0.000511	68.34%
C4($sp = 15$)	0.000120	92.54%
$Re = 600$		
$C(sp = \infty)$	0.002228	–
C1($sp = 35$)	0.000709	68.16%
C4($sp = 15$)	0.000109	95.12%

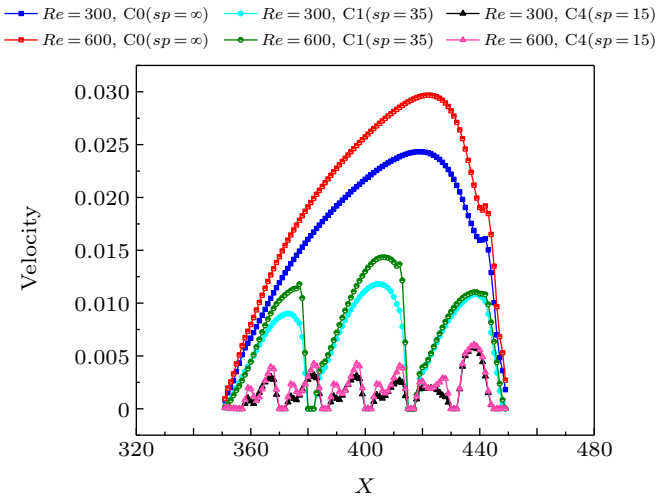


Fig. 5. Aneurysm neck velocity diagram of different stent shapes in the aneurysm under different Reynolds numbers.

Then the WSS of the aneurysm is considered. Figure 6 shows the comparison of the WSS of the aneurysm with different stent shapes when $Re = 300$ (Fig. 6(a)) and $Re = 600$

(Fig. 6(b)). It can be seen from Fig. 6 that the WSS at the corners of the aneurysm changes greatly, and the WSS at the right aneurysm corner of the aneurysm is significantly higher than that at the left aneurysm corner. The risk of rupture at the corner of the aneurysm is greater than that at the top of the aneurysm, and the risk of rupture at the right corner of the aneurysm is greater than that of the left corner. It can also be analyzed from Fig. 6 that the WSS at the corner of the aneurysm can be significantly improved after the intervention of the stent. The smaller the porosity of the stent, the smaller the WSS at the corner of the aneurysm.

Because of the large changes in the WSS at the left and right corners of the aneurysm, these places are more likely to contribute to the rupture of the aneurysm. Figure 7 shows the WSS at the left and right corners of the aneurysm when different stent shapes are inserted into the aneurysm under different Reynolds numbers. Comparing Figs. 7(a) and 7(b), it can be clearly seen that the WSS at the right corner of the aneurysm is greater. And the WSS at the corner of the aneurysm increases with the increase of the Reynolds number. After the intervention of the stent, the WSS at the corner of the aneurysm decreases, especially the improvement effect of the right corner of the aneurysm is obvious. The lower the porosity of the intervening stent, the smaller the WSS, and the smaller the impact of the WSS caused by the Reynolds number.

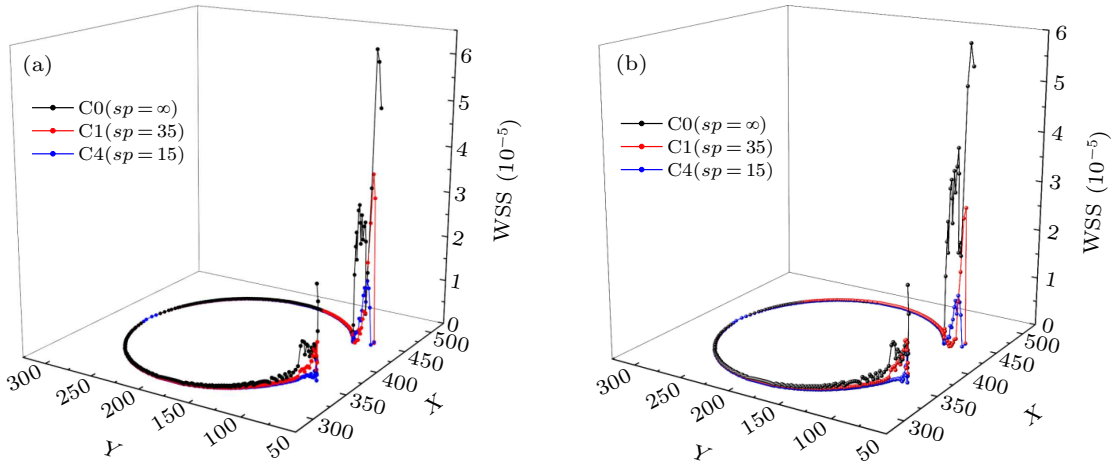


Fig. 6. Wall shear stress diagram of different stent shapes in the aneurysm under different Reynolds numbers: (a) $Re = 300$, (b) $Re = 600$.

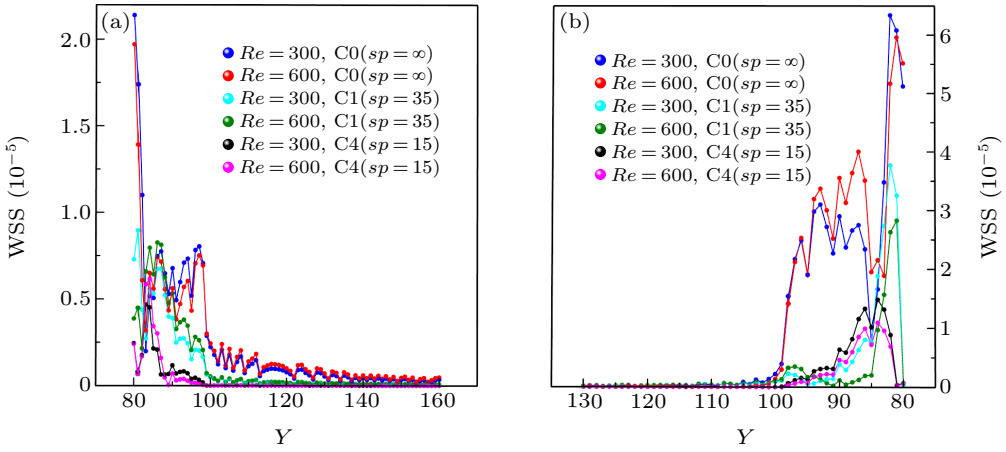


Fig. 7. Comparison of wall shear stress at the left and right corners of the aneurysm: (a) left corner, (b) right corner.

The analysis shows that the risk of aneurysm rupture is mainly centralized at the neck of the aneurysm, and the right aneurysm corner, that is, the position of the two aneurysm corners that is facing the direction of fluid, has a higher risk of rupture. When a person is in motion, the velocity and the WSS of the aneurysm are higher than those at rest. Interventional stent treatment in the aneurysm area can effectively reduce the velocity and WSS in the aneurysm, inhibit the formation of vortex, and reduce the risk of aneurysm rupture during strenuous exercise or emotional excitement. This highlights the significant advantages of stent interventional therapy.

3.2. Intra-aneurysm hemodynamic analysis of interventional double stent

Interventional stents are an effective treatment method to prevent aneurysm rupture, and the application of stent shape

optimization is still under exploration. In this section, a new stent form of double stent is considered. The Reynolds number is set as 300 in the simulation. And the C0, C2, C4, and C5 samples are used to compare the morphology of the dual stent with other intra-aneurysm stents to analyze the intra-aneurysm hemodynamics of the intervening dual stent.

Figure 8 shows the fluid velocity cloud diagram and flow pattern when different stent shapes are inserted into the aneurysms. Comparing Fig. 8(a) with Fig. 8(c), it can be seen that the speed of the aneurysm neck can be effectively improved after the intervention of the double-layer stent. From Figs. 8(b) and 8(c), it can be found that in the case of the same porosity, the inner streamline vortex center of the aneurysm with the double stent is moved upward. The velocity at the neck of the aneurysm improved better than that of the aneurysm neck with a single-layer stent ($sp = 30$).

Table 3 specifically shows the amount of intra-aneurysmal velocity reduction when different stent shapes such as double-layer stents are inserted. From Table 3, the intra-aneurysmal velocity reduction can reach 90.39% after the intervention of the dual stent. The effect of double stents on the blood flow velocity in the aneurysm is much better than that of single-layer stents with sp =30. And compared with the single-layer stent with sp =15, the intra-aneurysmal velocity reduction of the double stent and the single-layer stent is not much different. This reflects the advantages of double stents in preventing aneurysm rupture.

Table 3. Decrease of intra-aneurysm velocity with different stent forms.

	Average velocity V	Velocity reduction V_r
C0($sp = \infty$)	0.001616	–
C2($sp = 30$)	0.000440	72.76%
C5($sp = 30$-30)	0.000155	90.39%
C4($sp = 15$)	0.000120	92.54%

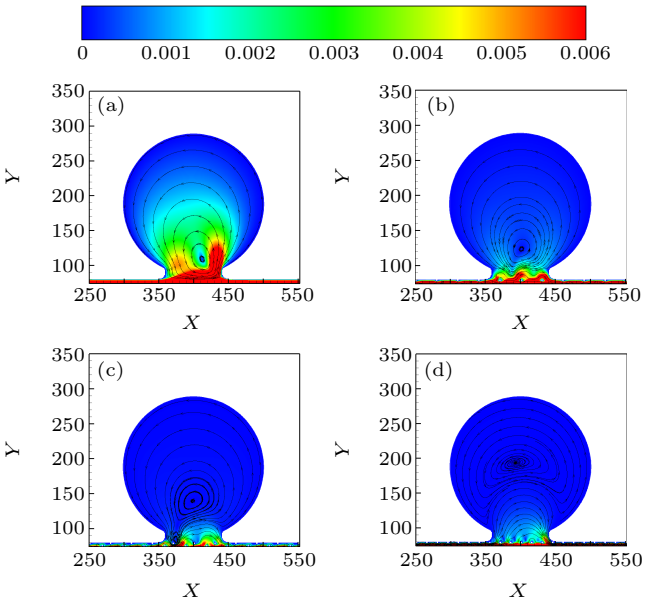


Fig. 8. The flow patterns of aneurysm without stent, with single stent and with double stent: (a) C0($sp = \infty$), (b) C2($sp = 30$), (c) C5($sp = 30$-30), (d) C4($sp = 15$).

Figure 9 shows the aneurysm neck velocity curves when there is no stent, single-layer stent, and double stent in the aneurysm. Consistent with the velocity cloud, the velocity at the neck of the aneurysm with dual stenting is lower than with single stenting of the same porosity ($sp = 30$), resulting in a lower risk of aneurysm rupture. When comparing the intra-aneurysmal intervention of a double stent and a single-layer stent with a lower porosity ($sp = 15$), it can be found that the speed of the two is similar at the right corner of the aneurysm. The analysis shows that at the right corner of the aneurysm where the risk of the rupture is greater, the intervention of a high-porosity double stent can basically achieve the effect of improving the flow rate when a low-porosity single-layer stent is inserted.

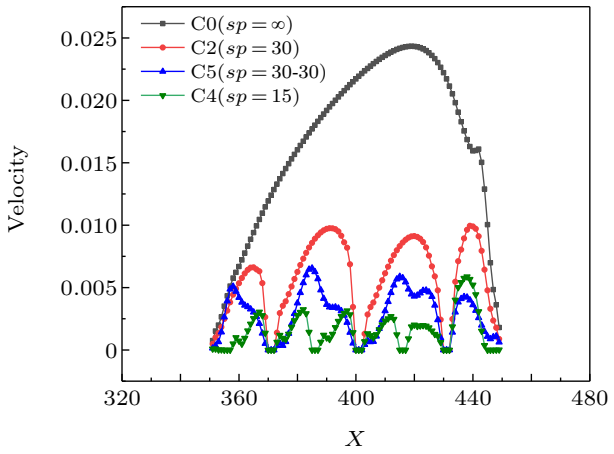


Fig. 9. Aneurysm neck velocity diagram of different stent shapes in the aneurysm.

Figure 10 shows the WSS at the left and right corners of the aneurysm when different stent shapes such as double-layer stents are inserted into the aneurysm. As seen in Fig. 10(b), also at the right aneurysm corner where the risk of aneurysm rupture is high, the WSS after intervention of the double stent is lower compared with that when a single-layer stent with the same porosity ($sp = 30$) is intervened. And the WSS after the intervention of double stent is not much different or even slightly lower than that of the intervention of single-layer stent with low porosity ($sp = 15$). Therefore, the intervention of the double stent can effectively reduce the deformation load of the aneurysm corners and reduce the possibility of aneurysm rupture.

It can be obtained that the intra-aneurysmal intervention effect of the double stent is better than that of the single-layer stent with the same porosity. The intra-aneurysmal velocity reduction after the intervention of double stents can reach 90.39%. And at the right corner of the aneurysm where the risk of rupture is greater, the double stent can even achieve the same intra-aneurysmal improvement effect as the low-porosity stent. This highlights the advantages of double stent interventional therapy for aneurysm.

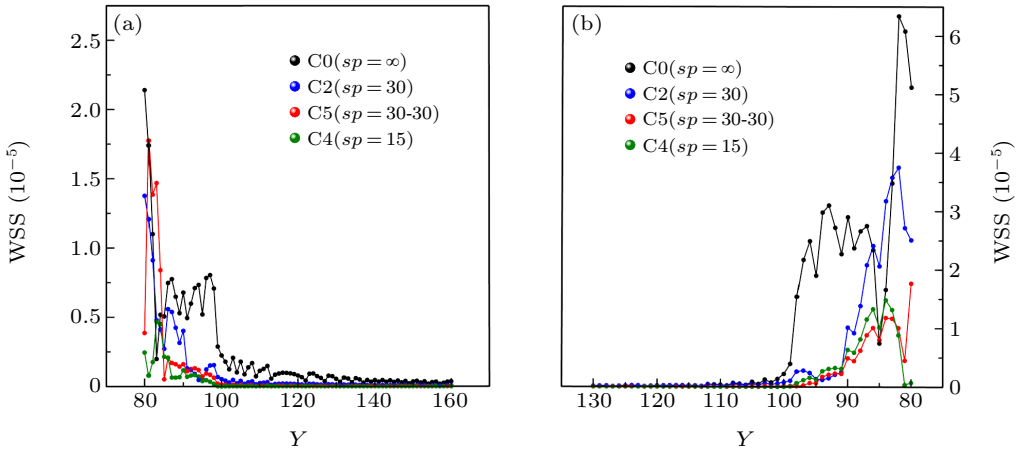


Fig. 10. Comparison of wall shear stress at the left and right corners of the aneurysm: (a) left corner, (b) right corner.

3.3. Intra-aneurysm hemodynamic analysis of interventional variable-spacing stent

In this section, another new type of stent, the variable pitch stent, is considered. The Reynolds number is set as 300 in the model. C0, C3, C6, C7, C8 samples are used, and the fixed aneurysm neck segment S is selected for the setting of the stent variation distance. The anterior stent densification (sp = 15-22-28-35), the middle stent densification (sp = 35-22-15-28), the posterior stent densification (sp = 35-28-22-15) and the isometric stent (sp = 25) are set up in the S segment for comparative analysis of intra-aneurysm hemodynamics.

Figure 11 shows the flow patterns when different variable-spacing stents are intervened in the aneurysm. It can be seen from the velocity cloud diagram in Fig. 11 that the stent with the front densification at the neck of the aneurysm (Fig. 11(b)) has a better effect on improving the velocity than other variable-spacing stents. However, the improvement effect of the dense stent in the middle part (Fig. 11(c)) and posterior part (Fig. 11(d)) on the aneurysm neck velocity is not obvious compared with the equal-spaced stent (Fig. 11(a)).

In Table 4, the average velocity reduction in the aneurysm is quantitatively analyzed when different variable-spacing stents are inserted. It can be seen that the velocity reduction can reach 80% when the stents with dense front and middle parts are inserted, which is slightly higher than the velocity reduction when the stents with equal spacing are inserted. However, when a stent with a dense posterior part is inserted, the velocity reduction is lower than that of an equally spaced stent, and the treatment effect of the stent becomes worse.

Table 4. Decrease of intra-aneurysm velocity with variable-spacing stents.

	Average velocity V	Velocity reduction V_r (%)
C0($sp=\infty$)	0.001616	–
C3($sp=25$)	0.000325	79.91%
C6(sp = 15-22-28-35)	0.000318	80.29%
C7(sp = 35-22-15-28)	0.000312	80.69%
C8(sp = 35-28-22-15)	0.000365	77.41%

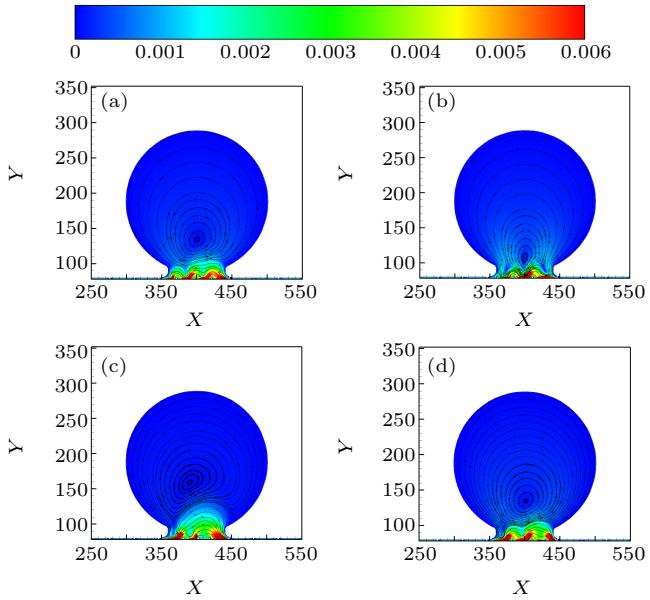


Fig. 11. The flow patterns of intra-aneurysmal intervention with different variable-spacing stents: (a) C3(sp = 25), (b) C6(sp = 15-22-28-35), (c) C7(sp = 35-22-15-28), (d) C8(sp = 35-28-22-15).

Figure 12 is a comparison diagram of aneurysm neck velocity when different variable-spacing stents are inserted into the aneurysm. It can be seen that the effect of taking different variable-spacing stents on the velocity distribution at the aneurysm neck varies greatly. When an anteriorly dense stent is intervened, the velocity near the left and right aneurysm corners of the aneurysm is smaller compared to when an isometric stent is intervened, reducing the probability of aneurysm rupture risk. Comparing the velocity curves when intervening in the central dense stent, the posterior dense stent and the isometric stent, it can be found that the velocity increases at the left and right aneurysm corners of the aneurysm, which is not conducive to the prevention of aneurysm rupture.

Figure 13 shows the WSS at the left and right aneurysm corners of the aneurysm for intra-aneurysmal intervention with different variable-spacing stents. It can be seen from Fig. 13 that the anterior densification stent can effectively reduce the

WSS at the left and right corners of the aneurysm, especially at the right corner where the risk of aneurysm rupture is greater (Fig. 13(b)). The improvement of WSS by anteriorly denser stents is better than that by equidistant stents. However, the intervention of a stent that becomes denser in the middle and denser at the back is not very effective in improving the WSS. In particular, at the right aneurysm corner, the WSS of the aneurysm is higher with the intervention of the mid-dense and posterior-dense stents than with the intervention of the isometric stents. Posterior densified stents are the least effective and tend to exacerbate aneurysm growth development and rupture.

Thus, it can be analyzed that the hemodynamic effects on the aneurysm are different for the intervention of different variable-spacing stents at the neck of the aneurysm. Among them, the anterior densified stent morphology is the most effective in preventing aneurysm rupture with an intra-aneurysmal velocity reduction of up to 80.29%. The central and posterior variably dense stent forms are not as effective in treating aneurysms.

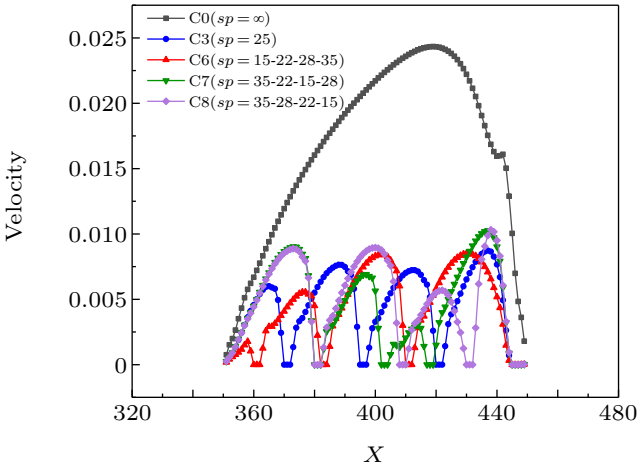


Fig. 12. Aneurysm neck velocity diagram of different variable-spacing stents in the aneurysm.

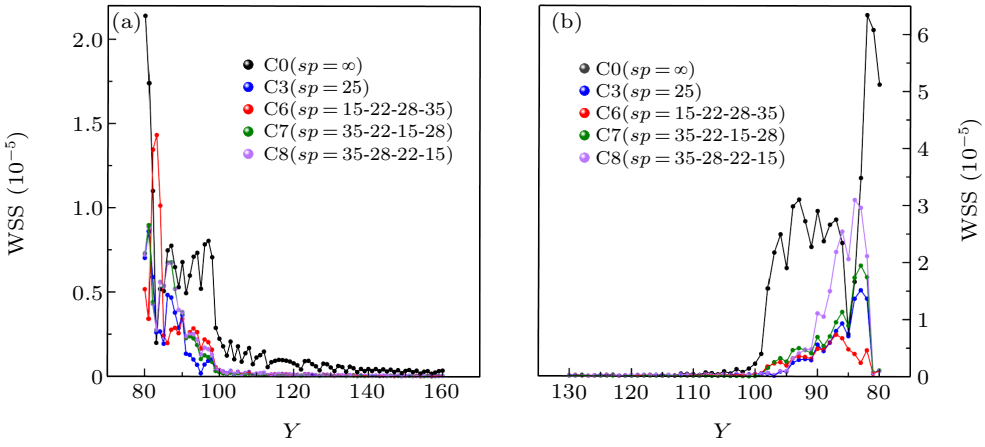


Fig. 13. Comparison of wall shear stress at the left and right corners of the aneurysm: (a) left corner, (b) right corner.

4. Conclusion

In this paper, LBM is used to study the hemodynamic mechanism in aneurysm. The flow characteristics of the ideal cerebral aneurysm model under different Reynolds number states when different stent shapes are inserted into the aneurysm are studied. At the same time, in view of the application problem of stent shape optimization, the feasibility of new stent shapes such as double stents and variable-spacing stents is explored. Hemodynamic factors such as velocity distribution characteristics and WSS of blood within the saccular aneurysm are analyzed. Based on the present results, some conclusions can be obtained:

(i) The risk of aneurysm rupture is mainly centralized at the neck of the aneurysm. And at the right corner of the aneurysm, that is, the position of the two corners facing the fluid is at a higher risk of rupture. When an aneurysm patient is in motion, the flow velocity and WSS in the aneurysm will be higher than those at rest. Interventional stenting in the aneurysm area is effective in reducing the velocity at the neck and WSS within the aneurysm, reducing the risk of aneurysm rupture during strenuous exercise or emotional stress.

(ii) The therapeutic effect of the double stent intervention in the aneurysm is better than that of the single-layer stent with the same porosity. Intra-aneurysmal velocity reduction after interventional double stenting is up to 90.39%. And at the right corner of the aneurysm where the risk of rupture is greater, the double stent can even achieve the same intra-aneurysmal improvement effect as the low-porosity stent. Therefore, double stents have certain advantages in the treatment of preventing aneurysm rupture.

(iii) The hemodynamic effects on the aneurysm are different when different variable-spacing stents are intervened for the aneurysm neck. Among them, anterior densification stents are the most effective in preventing aneurysm rupture with a velocity reduction of up to 80.29%, which can be considered for the treatment of aneurysms. In contrast, central and posterior variable density stents are not effective in the treatment of aneurysms, especially posterior variable density stents, which

should be avoided in the treatment.

Acknowledgment

Project supported by Management Project of General Hospital of Eastern Theater Command (Grant No. YYBJ2021043).

References

[1] Li Y P 2015 *Lattice Boltzmann numerical study on hemodynamics of tandem intracranial aneurysms*, MS Thesis (Wuhan: Huazhong University of Science and Technology) (in Chinese)
[2] Zhai X J, Amira A, Bensaali F, Al-Shibani A, Al-Nassr A, El-Sayed A, Eslami M, Dakua S P and Abinahed J 2019 *Phys. Rev. E* **31** e5184
[3] Detmer F J, Chung B J, Jimenez C, Hamzei-Sichani F, Kallmes D, Putman C and Cebral J R 2019 *Neuroradiology* **61** 275
[4] Xiang J P, Natarajan S K, Tremmel M, Ma D, Mocco J, Hopkins L N, Siddiqui A H, Levy E I and Meng H 2011 *Stroke* **42** 144
[5] Longo M, Granata F, Racchiusa S, Mormina E, Grasso G, Longo G M, Garufi G, Salpietro F M and Alafaci C 2017 *World Neurosurg.* **105** 632
[6] Sun Q, Growth A and Aach T 2012 *Med. Phys.* **39** 742
[7] Usmani A Y and Patel S 2018 *Int. J. Energy Clean Env.* **19** 119
[8] Meng H, Tutino V M, Xiang J and Siddiqui A 2014 *Am. J. Neuroradiol* **35** 1254
[9] Longo M, Granata F, Racchiusa S, Mormina E, Grasso G, Longo G M, Garufi G, Salpietro F M and Alafaci C 2017 *World Neurosurg.* **105** 632
[10] Paisal M S A, Taib I and Ismai A E 2017 *IOP Conference Series: Materials Science and Engineering* **165** 012003
[11] Yadollahi-Farsani H, Scougal E, Herrmann M, Wei W, Frakes D and Chong B 2019 *Comput. Methods Biomech. Biomed. Eng.* **22** 961
[12] Molyneux A J, Kerr R S, Birks J, Ramzi N, Yarnold J, Sneade M and Rischmiller J 2009 *Lancet Neurol.* **8** 427
[13] Zhang P, Sun A Q, Zhan F, Luan J Y and Deng X Y 2014 *J. Biomech.* **47** 3524
[14] Suri H, Ionita C N, Baier R E and Rudin S 2011 *IEEE Engineering in Medicine and Biology Society Conference Proceedings*, August 30–September 3, 2011, Boston, USA, p. 1105
[15] Chen C, Xiong Y, Jiang W T, Wang Y B, Wang Z Z and Chen Y 2020 *Cardiovasc. Eng. Technol.* **11** 36
[16] Li Y J, Verrelli D I, Yang W, Qian Y and Chong W 2020 *J. Biomech.* **100** 109590
[17] He Y L, Wang Y and Li Q 2008 *Lattice Boltzmann Method: Theory and Applications* (Beijing: Science Press) pp. 1–9 (in Chinese)
[18] Guo Z Y and Zheng C G 2009 *Theory and Applications of Lattice Boltzmann Method* (Beijing: Science Press) pp. 1–15 (in Chinese)
[19] Krüger T, Kusumaatmaja H, Kuzmin A, Shardt O, Silva G and Viggen E M 2017 *The Lattice Boltzmann Method* (Berlin: Springer) pp. 54–56
[20] Wen B H, Liu H Y, Zhang C Y and Wang Q 2009 *Chin. Phys. B* **18** 4353
[21] Yi H H, Yang X F, Wang C F and Li H B 2009 *Chin. Phys. B* **18** 2878
[22] Yun B M, Dasi L P, Aidun C K and Yoganathan A P 2014 *J. Fluid Mech.* **754** 122
[23] Wang Y, Navarro L, Zhang Y, Kao E, Zhu Y M and Courbebaisse G 2017 *Comput. Sci. Eng.* **19** 56
[24] Kang X Y, Ji Y P, Liu D H and Jin Y J 2008 *Chin. Phys. B* **17** 1041
[25] Osaki S, Hayashi K, Kimura H, Seta T, Kohmura E and Tomiyama A 2019 *Comput. Math. Appl.* **78** 2746
[26] Afrouzi H H, Ahmadian M, Hosseini M, Arasteh H, Toghraie D and Rostami S 2020 *Comput. Method Programs Biomed.* **187** 105312
[27] Czaja B, Závodszky G, Tarksalooyeh V A and Hoekstra A G 2018 *J. R. Soc. Interface* **15** 20180485
[28] Li S, Latt J and Chopard B 2018 *Comput. Fluids* **172** 651
[29] Li S, Chopard B and Latt J 2019 *J. Comput. Sci.* **38** 101045
[30] Li S, Latt J and Chopard B 2018 *Int. J. Numer. Method Biomed.* **34** e2949
[31] Zhang Y, Wang Y, Kao E, Florez-Valencia L and Courbebaisse G 2019 *J. Biomech.* **82** 20
[32] Guo Z L, Shi B C and Wang N C 2000 *J. Comput. Phys.* **165** 288
[33] Matyka M, Koza Z and Mirosław L 2013 *Comput. Fluids* **73** 115
[34] Hirabayashi M, Ohta M, Rüfenacht D A and Chopard B 2004 *Futur. Gener. Comp. Syst.* **20** 925
[35] Zou Q S and He X Y 1997 *Phys. Fluids* **9** 1591